Design considerations in high-sensitivity off-axis integrated cavity output spectroscopy

Article *in* Applied Physics B · September 2008

DOI: 10.1007/s00340-008-3137-9

Appl. Phys. B 92, 467–474 (2008)
DOI: 10.1007/s00340-008-3137-9

Applied Physics B
Lasers and Optics

E.J. MOYER[1,✉]
D.S. SAYRES[2]
G.S. ENGEL[3]
J.M. ST. CLAIR[4]
F.N. KEUTSCH[5]
N.T. ALLEN[2]
J.H. KROLL[6]
J.G. ANDERSON[2]

Design considerations in high-sensitivity off-axis integrated cavity output spectroscopy

[1] Dept. of the Geophysical Sciences, University of Chicago, 5734 S. Ellis Ave., Chicago, IL 60637, USA
[2] Dept. of Chemistry and Chemical Biology, Harvard University, 12 Oxford St., Cambridge, MA 02138, USA
[3] Dept. of Chemistry, University of Chicago, 927 E 57th St., Chicago, IL 60637, USA
[4] Dept. of Geological and Planetary Sciences, California Institute of Technology, 1200 E California Blvd., Pasadena, CA 91125, USA
[5] Dept. of Chemistry, University of Wisconsin-Madison, 1101 University Ave., Madison, WI 53706, USA
[6] Aerodyne Research, 45 Manning Rd., Billerica, MA 01821, USA

Received: 20 March 2008/Revised version: 10 July 2008
Published online: 16 August 2008 •

ABSTRACT Off-axis integrated cavity output spectroscopy (OA-ICOS) has generated much interest because it potentially allows highly sensitive field measurements with robust optical alignment. We discuss here design choices involved in design of an OA-ICOS instrument and how these choices impact instrument sensitivity, using as our example the design of the Harvard ICOS isotope instrument, which demonstrates the highest reported sensitivity for mid-IR OA-ICOS (2.4×10^{-11} cm^{-1}Hz$^{-1/2}$ at 6.7 μm, obtained during measurements of water vapor isotopologues H_2O, HDO, and $H_2\,{}^{18}O$ in the laboratory and onboard NASA's WB-57 high-altitude research aircraft). We compare the sensitivity of several OA-ICOS instruments with differing design parameters, show how comparisons are hindered by differing definitions of instrument performance metrics, and suggest a common metric of $\mathrm{MDA}_{\mathrm{meas}}$, the fractional absorption equivalent to 1σ uncertainty in an actual measurement, normalized to 1 s integration. We also note that despite an emphasis on sensitivity in the literature, in the Harvard ICOS isotope instrument and likely also similar instruments, systematic errors associated with fitting of the baseline laser power are of equal importance to total measurement uncertainty.

1 Introduction

Since its development a decade ago [1, 2], integrated cavity output spectroscopy (ICOS, or alternatively, CEAS for "cavity-enhanced absorption spectroscopy") has generated strong interest among the spectroscopic community for its longer optical path and promise of correspondingly higher sensitivities. Traditional tunable diode laser absorption spectroscopy (TDLAS) using multipass Herriott or White cells is limited to pathlengths of ≈ 100 m. ICOS, in which narrowband cw laser light is trapped in highly reflective optical cavities for up to tens of microseconds, can produce effective optical pathlengths of several to tens of km in the mid-IR and near-IR, respectively. (Maximum mirror reflectivities are higher in the near-IR). The introduction of off-axis alignment permitted the use of ICOS for field measurements by allowing less stringent stability requirements [3]. Off-axis alignment removes the need to lock the cavity to the laser wavelength by producing a dense mode structure such that even narrow-band lasers ($\Delta\nu < 1$ MHz) couple to many cavity modes simultaneously. The result is alignment robustness at the cost of a steep reduction in cavity throughput power, a tradeoff that is nevertheless acceptable for many industrial and scientific applications.

In recent years numerous groups have explored the use of off-axis ICOS (OA-ICOS) (e.g. [4–10]). One factor driving interest in the technique is the increasing use of optical spectroscopy for measuring the isotopic composition of gas-phase species (e.g., [11–19]). Isotopically substituted molecules are some 100–10 000 times less abundant than the most common isotopologues and fractional measurement uncertainties must often be $< 0.01\% - 1\%$ (depending on the species) to be scientifically useful. Isotopic measurements therefore place a premium on sensitivity, making high-finesse cavity based techniques such as OA-ICOS appealing for isotopic studies [7, 9, 16].

We discuss here the design decisions involved in achieving high-sensitivity OA-ICOS measurements and in particular the design of a new instrument, the Harvard ICOS isotope instrument (henceforth "Harvard ICOS"). Harvard ICOS uses OA-ICOS for the measurement of water vapor isotopic composition, making simultaneous measurements of H_2O, HDO, and $H_2\,{}^{18}O$ [20]. We use comparisons with several other OA-ICOS instruments to highlight how design choices affect overall sensitivity (Sect. 5). We also discuss additional factors that may be more important than sensitivity in determining total measurement uncertainty (Sect. 4).

2 Off-axis ICOS

The OA-ICOS technique has been reviewed extensively in the literature (e.g. [3, 4]). We highlight here only some of the most relevant aspects for achieving high sensitivity. Briefly, as in all cw cavity-enhanced techniques, a narrowband cw laser is injected into a closed optical cavity formed by a pair of high-reflectivity mirrors and tuned over an absorption feature of interest. The optical pathlength of the resulting absorption spectrum can be thought of as the distance that light travels during the mean residence time τ of a photon in the

✉ Fax: +1.773.702.9505, E-mail: moyer@uchicago.edu

optical cavity

$$\tau = \frac{L}{c(1-R+\alpha L)}\,, \tag{1}$$

where R is the mirror reflectivity and α the per-pass intracavity absorption. Effective optical pathlength is then

$$L_{\text{eff}} = \frac{L}{(1-R+\alpha L)}\,. \tag{2}$$

The resultant gain factor can be large. With 200 ppm mirrors ($R = 99.98\%$) and an evacuated cavity ($\alpha = 0$), the gain factor is $1/(1-R) = 5000$, and a one-meter optical cell would yield an effective pathlength of 5 km.

The presence of an absorber lowers the cavity gain and therefore the effective pathlength. If peak αL is significant compared to $(1-R)$, an OA-ICOS absorption spectrum is not described by the Beer–Lambert law but has a broader lineshape with linecenter absorption depressed relative to the wings. Absorption features will also be skewed if the laser scan rate is high enough that the time to sweep across a spectral line is comparable to the cavity time constant. However, spectra can be accurately fit and concentrations retrieved even for quite severe skews. (See [20] for a discussion of fitting algorithms).

In OA-ICOS, light is injected off-axis to alter the resonance properties of the cavity, allowing simultaneous pumping of many transverse modes to produce a dense cavity mode spectrum. It can also be instructive to think of a cavity with an ideal Herriott or Lissajous pattern with spatial separation of successive passes as a folded cavity of length nL, where n is the number of passes before the reentrant condition is attained [21]. The effective cavity free spectral range then becomes $\text{FSR}_{\text{eff}} = c/(2nL)$. In the limit of small overlap between spots, these two views are equivalent, and the simplified picture has predictive value for understanding resultant mode spectra. Note that while effective optical pathlength is determined by mirror reflectivity and cell length, cavity FSR_{eff} is a function of alignment: $n \neq 1/(1-R)$. The aim of off-axis alignment in OA-ICOS is to reduce cavity FSR_{eff} to well below the laser linewidth so that variations in coupling over the duration of the scan become negligible.

In practice, the goal of perfectly non-resonant coupling is not achieved. Fluctuations in laser coupling are in fact the dominant limitation on spectroscopic sensitivity in most OA-ICOS experiments. These spurious cavity resonances are not stable with wavelength but result from laser phase noise and/or mechanical instability of the cavity [6, 22]. The resultant "optical noise" is tractable by signal averaging.

Because an OA-ICOS cell is largely non-resonant, any attempt to increase effective optical pathlength by use of higher-reflectivity mirrors necessarily comes at the expense of power incident on the detector. The power transmitted through a cavity in a perfectly non-resonant configuration would be

$$I = I_0 \frac{1}{2} T\,, \tag{3}$$

where T is the mirror transmission and the factor of two results from the loss of light through both front and rear mirrors. In the limit that absorptive losses are negligible, $T = 1-R$ and

$$I \approx I_0 \frac{1}{2}(1-R)\,, \tag{4}$$

meaning transmitted power is reduced by the same gain factor that boosts effective pathlength. In practice, absorptive losses are often comparable to transmission, producing still greater reduction in power at the detector.

3 Design choices and tradeoffs

Design of OA-ICOS instruments involves consideration of many factors, including cost, weight, robustness, accuracy, ease of use, and sensitivity. In the design of Harvard ICOS, the overwhelming priority was sensitivity, because the limiting molecule in the target measurement, HDO, has mixing ratios of < 1 ppbv in the dry stratosphere. Because design decisions were made almost solely with this goal in mind, this experiment serves as a useful example for exploring the instrumental tradeoffs associated with sensitivity. The basic configuration of Harvard ICOS is typical of OA-ICOS experiments (Fig. 1), so considerations undertaken during its design will be broadly applicable to other OA-ICOS instruments.

The resulting choices for Harvard ICOS are somewhat different from those made by most OA-ICOS users, notably a more aggressive scan rate and a reduced contribution of optical noise relative to detector and electronic noise. Although most published OA-ICOS experiments to date are configured such that optical noise is the dominant limitation and detector and electronic noise insignificant, we found that optimal measurement sensitivity was achieved when the two noise

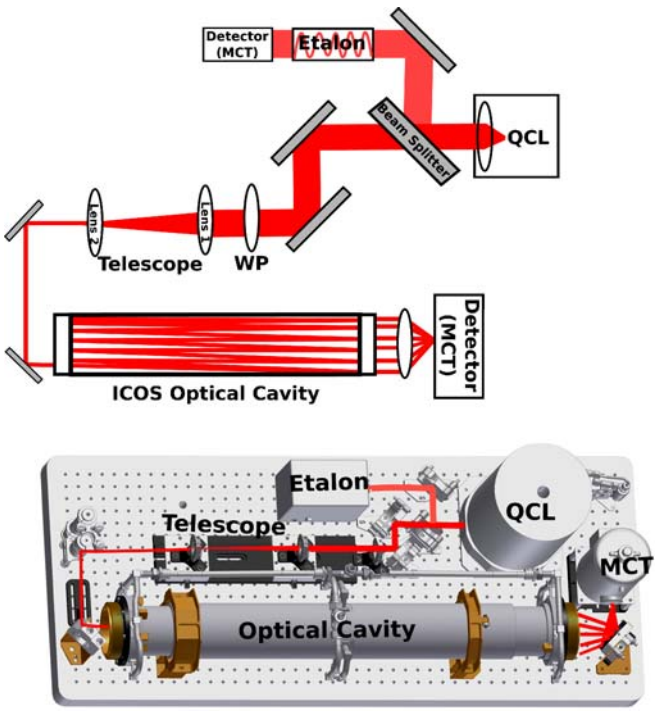

FIGURE 1 Schematic of the optical layout of the Harvard ICOS Isotope Instrument, which is typical of OA-ICOS experiments (*top*). Drawing of the resulting field instrument (*bottom*)

sources were approximately equal. Design tradeoffs involving loss of power at the detector then became important.

3.1 *Instrument description*

The Harvard ICOS light source is a liquid-nitrogen-cooled cooled cw quantum cascade laser (QCL) producing ≈ 35 mW output power at 6.7 μm (Alpes Lasers). Light from the QCL is collimated by an internal lens and passes through a beam splitter, with a fraction diverted to a diagnostic Ge etalon (free spectral range 0.0198 cm^{-1}) used as a frequency reference. The majority of the light is beam-shaped by a telescope and directed into an optical cavity consisting of two spherical ZnSe mirrors of radius of curvature 140 cm ($R = 99.98\%$ or $(1 - R) \approx 215$–235 ppm, coating by Lohnstar Optics) mounted 90 cm apart for a d/f of 1.3, optimized for minimizing beam interferences. (Note that R, although constant during a data run, varies somewhat with efficacy of cleaning after the cell has been opened). Light exiting the cavity is focused onto a liquid-nitrogen-cooled HgCdTe detector (Kolmar Technologies). A quarter-wave plate (labeled "WP" in Fig. 1) functions as an optical isolator to minimize feedback into the laser. In the experiments described here, the laser is current-tuned over a wide scan, 1.5 cm^{-1}, to measure multiple lines of water isotopologues (H_2O, HDO, and $H_2^{18}O$) as well as CH_4. All control and signal-processing electronics were built in-house.

In its field use, the OA-ICOS based instrument was mounted on NASA's WB-57 high-altitude aircraft and flown to altitudes of 18 km, drawing ambient air into the optical cell and making in-situ measurements of gas-phase water. When sampling, cell pressure is maintained at 40 Torr and gas temperature at 25 °C, with temperature gradients across the cell at < 0.5 °C. (During the lowermost altitudes on ascent and descent, the cell is sealed and filled with dry nitrogen to protect the mirrors). The instrument was flown on NASA-sponsored science campaigns between 2005–2007. The experimental configuration, flight instrument, sampling strategy, and fit algorithms are described in more detail in [20, 23].

3.2 *Laser source and wavelength*

If an OA-ICOS experiment is to make use of long optical pathlength, it must also use a high-power light source, since the higher the mirror reflectivity, the lower the cavity throughput. During the design phase of the experiment described here, cw diode lasers of reasonably high power (tens to hundreds of mW) were available at only one fundamental ro-vibrational water band, ν_2 at 6.7 μm. Measurements could also be made with near-IR DFBs in various combination and overtone bands. Near-IR DFB beam quality is far better, mirror coatings can be made more reflective, and near-IR InGaAs detectors ($D^* > 1 \times 10^{12}$ Jones) are also better than mid-IR HgCdTe detectors ($D^* \approx 7 \times 10^{10}$ Jones). It is unlikely that any experiment using mid-IR QC lasers can match the best intrinsic sensitivity reported in the near-IR (e.g. [6]). Nevertheless, the strength of molecular absorption lines in the ν_2 fundamental is an order of magnitude greater than those in combination bands. We estimated that we should choose the mid-IR if spectroscopic sensitivity could be kept to within an order of magnitude of that for near-IR OA-ICOS.

3.3 *Mirror and detector size*

Spurious resonant couplings that produce optical "noise" increase when beams in the optical cavity overlap, reducing the cavity FSR_{eff}. Larger mirrors that allow a larger beam pattern footprint therefore allow reduced optical resonance noise. A larger beam pattern, however, requires a larger detector (or suffers greater power loss), because cavity output cannot be perfectly focused. As larger detectors have intrinsically lower detectivity, mirror size cannot increase indefinitely: at some point detector and electronic noise will become the dominant limitation. The optimum tradeoff must be evaluated for each experiment or instrument. With the 6.7 μm QC lasers used in these experiments, whose beam quality was relatively poor, instrument design was driven toward very large mirrors to accommodate a large beam pattern. After testing a variety of mirror diameters, we settled on 4″, with a corresponding 4″ diameter ZnSe focusing lens and a custom-built 3 mm HgCdTe detector. Even with a detector of this size, we capture only some 50% of the output light from the far mirror of the cavity.

3.4 *Mirror reflectivity*

As discussed above, OA-ICOS involves an inevitable tradeoff between optical pathlength and transmitted power, and therefore between absorption depth and detector and electronic noise relative to signal. In the hypothetical case of perfectly transmissive optical cavity mirrors, the relative contribution of detector and electronic noise would be independent of mirror reflectivity: per-pass noise-equivalent-absorption due to these noise sources alone, A_{det}, would be constant for all R. In practice, mirrors have finite absorptive losses and

$$A_{det} \propto ((1 - R)/T)^2 = 1/(FT)^2 , \tag{5}$$

where FT is the fraction of mirror loss that is transmitted. In dielectric coated mirrors, R increases and FT decreases with the number of coating layers, so A_{det} increases with reflectivity. Use of more reflective cell mirrors is then counterproductive if detector and electronic noise dominate.

In the OA-ICOS configuration described here, optical noise was sufficiently low that detector and electronic noise were a significant limiting factor and this tradeoff was of importance. The mirror design for the experiment was tailored accordingly, reducing the number of coating layers from an initial 10 to 9 to increase FT at the expense of reflectivity. (As $(1 - R)$ increased from ≈ 160 ppm to ≈ 215 ppm, FT increased from $\approx 45\%$ to $\approx 70\%$, giving us a 60% reduction in A_{det}). The optimal mirror coating for a given OA-ICOS experiment will depend on the particular laser, detector, and mirrors used.

3.5 *Scan rate*

The optical resonances that limit sensitivity require time to build up in the cavity. Faster scanning therefore reduces optical noise, but faster scanning also increases skew on the resulting spectral features. We found optimal measurement sensitivity at scan rates that were aggressive compared

to those of most OA-ICOS users, scanning over the FWHM of a spectral line in some three cavity time constants

$$\tau_{\text{line}} \approx 3\tau \tag{6}$$

or

$$f_{\text{line}} \approx 0.3 f_{\text{cav}}\,, \tag{7}$$

where e.g. $f_{\text{cav}} = 1/(2\pi\tau)$. We then oversample the resulting skewed spectral lines strongly. The tradeoff in reduced optical noise warrants these scan rates as it exceeds any decrease in fit precision due to line skew.

4 Measurements and results

Implementation of this design resulted in achievement of satisfactory sensitivity for measurement goals. In final configuration, in both laboratory and flight we routinely achieved a noise-equivalent absorption sensitivity (NEAS) of 2.4×10^{-11} cm^{-1}Hz$^{-1/2}$ (Fig. 2) [20]. This sensitivity is less than the maximum achieved in near-IR OA-ICOS but is the highest reported for mid-IR OA-ICOS. The achieved NEAS corresponds to a 1 s minimum detectable absorption during a normal scan (MDA$_{\text{ps}}$) of 3.6×10^{-4}. In good alignment conditions, integration to over 100 s is possible with noise suppression characteristic of white noise (Fig. 3).

Measurement precision is consistent with this inferred sensitivity, though it is determined not from NEAS but from fitting of spectra from calibration runs at a variety of water vapor concentrations (Fig. 4). Laboratory calibrations give a 1σ instrument measurement precision of ± 0.20 ppbv for HDO and 0.28 ppmv for H_2O, equivalent to fractional absorptions of 3.6 and 4.2×10^{-4}, respectively. Measurement precision for H_2O is hampered by the necessity of choosing an H_2O line with linestrength some 1000 times less than the maximum in this absorption band to more closely match the absorption of less-abundant HDO. (See Sect. 5 for a discussion of the relationship between MDA$_{\text{ps}}$ and measurement precision,

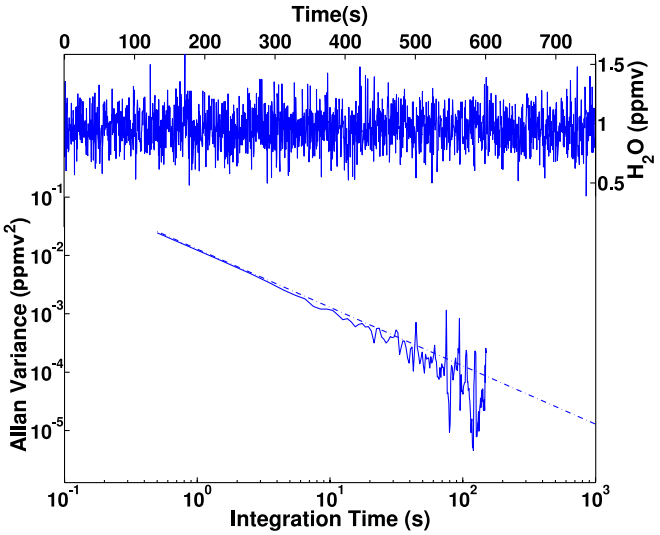

FIGURE 3 Allan variance plot showing the decrease in Harvard ICOS signal variance as a function of integration time for laboratory measurements of 1 ppmv H_2O in good alignment conditions. The dash-dot line represents the theoretical white noise line ($1/n$). Poor alignment can reduce the efficacy of integration

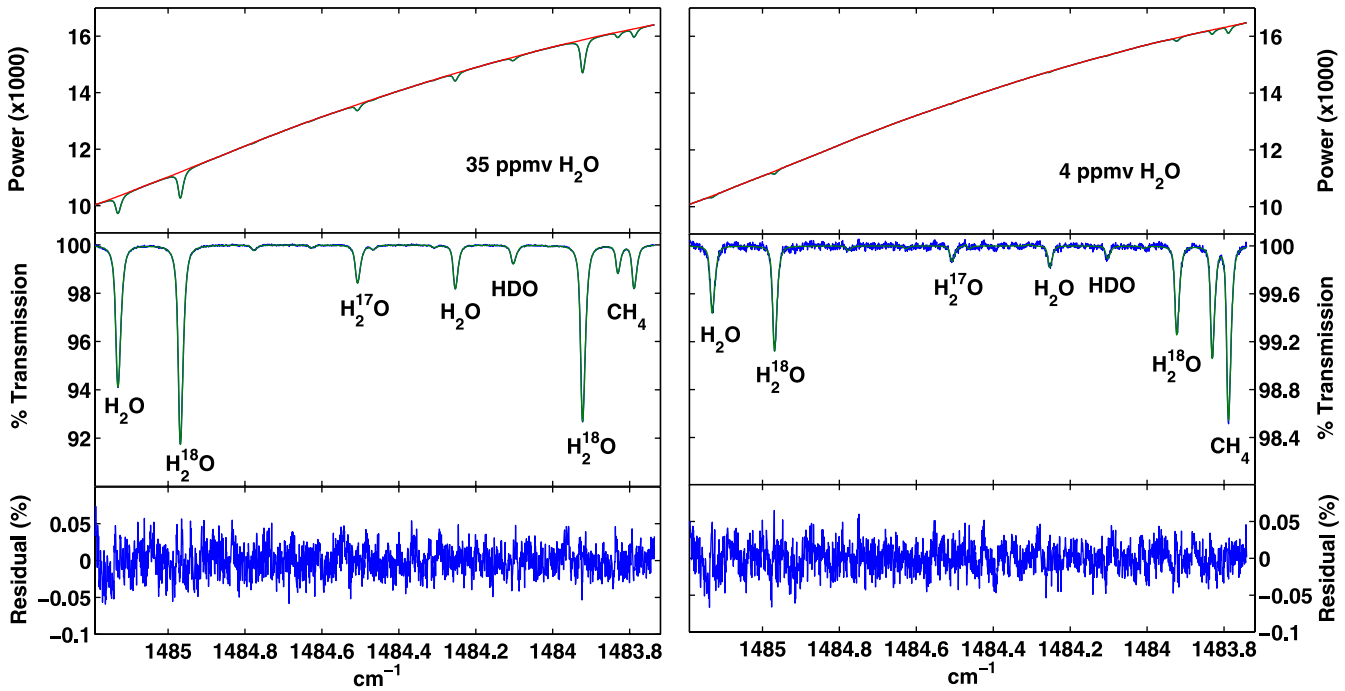

FIGURE 2 Fits of data at 35 ppmv H_2O (*left plots*) and 4 ppmv H_2O (*right plots*), 4 s integration. *Top*: raw data, fit, and derived baseline in blue, green, and red respectively. *Middle*: data with baseline removed, plotted in units of percent transmission. Note that the range of the y-axis is not the same for both plots. *Bottom*: the residual from the fit also in units of percent transmission. The fit residual for these 4 s data is $\sigma = 1.8 \times 10^{-4}$ or MDA$_{\text{ps}} = 3.6 \times 10^{-4}$. In this data run, $R = 227$ ppm so that $L_{\text{eff}} = 3.96$ km. The raw sample rate is 625 kHz and scan rate 113 Hz, with co-adding of adjacent data points to yield 2765 points across the scan. From (19), NEAS $= \text{MDA}_{\text{ps}}\sqrt{2}/(L_{\text{eff}}\sqrt{\#\text{pts}}) = 2.4 \times 10^{-11}$

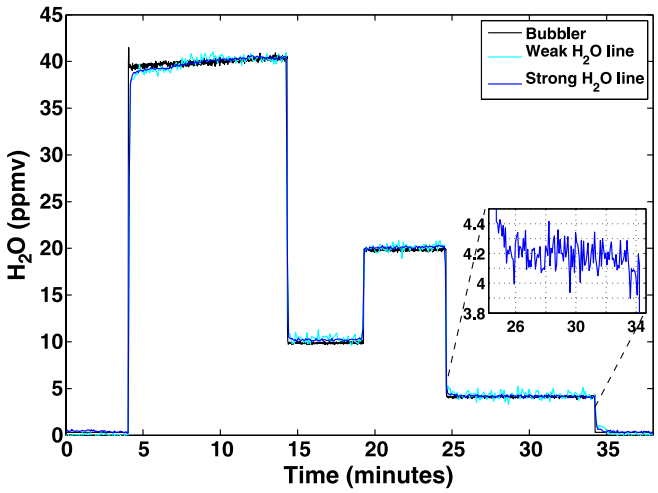

FIGURE 4 Sample calibration run from which measurement precision is determined. Input water vapor mixing ratio is shown in *black* and measurements of strong and weak water absorptions in *blue* and *cyan* respectively. The *enlargement* of a 4 ppmv segment shows the intrinsic measurement precision. Slight hysteresis can be seen at the beginning of the 40 ppmv segment. Total measurement uncertainty will include both hysteresis effects and systematic errors in spectroscopic fits

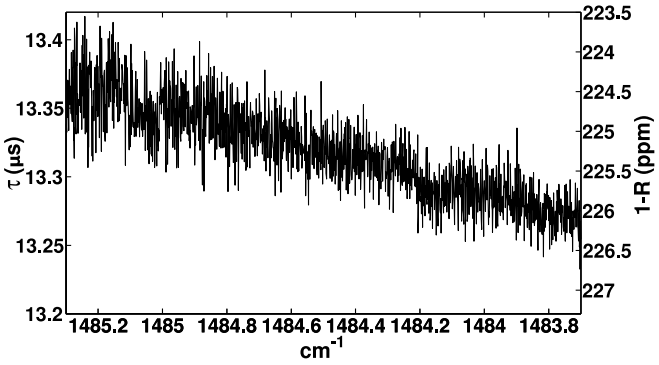

FIGURE 5 Reflectivity curve of the cavity mirrors, measured using ringdown, as a function of frequency. The cavity time constant, τ, varies by 1% over the frequency range scanned by the laser. This variation would translate into a $\pm 0.5\%$ error in concentration for absorptions at either end of the scan if the reflectivity were measured only at the mean laser frequency

definitions of MDA_{ps} and NEAS, and comparison with other published work).

We emphasize that neither MDA nor NEAS is sufficient to characterize a spectroscopic instrument and that reliance on these metrics may be deceptive. An equally important limiting factor is the ability of the fit to represent baseline power fluctuations across the scan. These include both the laser base power curve and semi-stable etalons due to reflections in and between instrument optics, including the cell mirrors themselves. In Harvard ICOS, and likely also other instruments, potential measurement bias due to these factors is comparable to the measurement precision stated above [20]. These systematic errors may vary slowly during field use on timescales of minutes to hours, beyond the integration time horizon.

Several additional factors make minimal contribution to measurement uncertainty in Harvard ICOS only because of careful treatment. The nonlinear tuning rate across the scan is monitored continuously via the Ge etalon. Variations in mirror reflectivity across the scan, which are significant, are measured by cavity ringdown by evacuating the cell and pulsing the laser at gradually increasing current. Although the target spectral region falls near the peak of the mirror reflectivity curve, R nevertheless varies by some 2 ppm across the 1.5 cm^{-1} spectrum (Fig. 5). During data acquisition, mirror reflectivity is monitored by this protocol at the beginning and end of each data run (in the laboratory) or aircraft flight (in field use), but degradation of reflectivity during a single flight is undetectable. Degradation of alignment during aircraft use with concomitant changes in external pressure is a more serious danger, and must be minimized by aligning the cell via a systematic procedure that checks robustness at a variety of cell pressures. We highlight these issues only because failure to account for them would lead to systematic error difficult to empirically calibrate.

Although this paper focuses almost entirely on sensitivity, it should be noted that in the development effort for Harvard ICOS, work on the fit algorithm, instrument operation protocol, and instrument design to combat systematic errors occupied as much time as did initial work on optical configuration to minimize NEAS. It cannot be overemphasized that slow-varying systematic errors are the likely limiting factor in the use of OA-ICOS for scientific measurements.

5 Comparisons of experiments and instruments

From the published literature, the results here appear to be the most sensitive mid-IR OA-ICOS measurements yet made. Comparisons of spectroscopic instruments and laboratory experiments are, however, hindered by the use of different metrics for evaluating performance. The same metric may also be defined differently by different authors. We discuss here two often-cited metrics: "minimum detectable absorption" (MDA, with units of $Hz^{-1/2}$) and "noise equivalent absorption sensitivity" (NEAS, with units of $cm^{-1}Hz^{-1/2}$). Authors vary in their definitions of these terms, in normalization standards, and in decisions on which bandwidths are relevant.

The first two differences are relatively straightforward, though lending some surface confusion to the literature. Although MDA is generally taken to be inclusive of optical pathlength and therefore with units of $Hz^{-1/2}$, "minimum detectable absorption" is sometimes cited with units of $cm^{-1}Hz^{-1/2}$ [24] or even ppmv $Hz^{-1/2}$ (molecular concentration) [25]. And although most authors normalize to 1 s integration, others define MDA as minimum detectable absorption in the integration time of a typical measurement [26]. An integration time of 30 s, for example, will in this definition yield an MDA lower by a factor of five from normalized MDA. Some experimenters further scale MDA by the number of optical passes, giving a "per pass" value that is reduced by the cavity gain factor $1/(1-R)$ [3, 4, 25]. For mirror losses of 400–40 ppm, this scaling reduces MDA by a factor of 2500–25 000.

More fundamentally, authors disagree on the relevant bandwidth for use in calculating MDA and NEAS. Comparison of OA-ICOS experiments is complicated by the existence of multiple relevant signal bandwidths and timescales: the bandwidth of the detector + preamp system bw_{det}, the data

acquisition rate r_{data} and corresponding Nyquist frequency $f_{\mathrm{acq}} = r_{\mathrm{data}}/2$, and the cavity frequency $f_{\mathrm{cav}} = 1/(2\pi\tau)$. The frequencies must be considered relative to that of the signal being detected – the absorption line – which is in turn a function of the scan length and scan rate f_{scan}. We define the "line frequency" as $f_{\mathrm{line}} = 1/(2\pi\tau_{\mathrm{line}})$, where τ_{line} is the time required to scan across the FWHM of a single absorption feature. These various bandwidths affect the signal in different ways. A low-pass preamp at the end of the signal chain, for example, filters the entire signal, but the optical cavity filters optical resonances only and has no effect on downstream detector and electronic noise (an important distinction in optical configurations like ours where the two noise sources are comparable).

The various system frequencies may differ by an order of magnitude in a single OA-ICOS experiment or between different experiments. The diversity of OA-ICOS optical configurations in the published literature is striking. In the instrument described in this paper,

$$bw_{\mathrm{det}} > f_{\mathrm{acq}} \gg f_{\mathrm{cav}} \approx f_{\mathrm{line}}\,. \tag{8}$$

We scan rapidly relative to the cavity time constant and oversample the resulting spectra, recording some 20 datapoints across the FWHM of an absorption line in a time period of less than three cavity time constants.

In the experiments of Kasyutich et al. [7],

$$bw_{\mathrm{det}} > f_{\mathrm{acq}} > f_{\mathrm{cav}} \gg f_{\mathrm{line}}\,, \tag{9}$$

the authors scan slowly relative to the cavity time constant (τ), so that lines are nearly unskewed, but again oversample relative to τ.

Finally, in the early work of Paul et al. [3] and recent work of Malara et al. [24],

$$f_{\mathrm{cav}} > f_{\mathrm{acq}} \gg f_{\mathrm{line}}\,. \tag{10}$$

The authors both scan and acquire data slowly relative to the cavity frequency, so that skew is minimal and every recorded datapoint is independent. (The authors do not specify bw_{det}, but it is presumably $> f_{\mathrm{cav}}$).

Determining the optimal choice of parameters is not simple and we do not claim to have done so definitively. Rapid scanning with $f_{\mathrm{cav}} \approx f_{\mathrm{line}}$ does complicate signal processing but benefits signal since, as noted before, the larger f_{line}, the greater the suppression of optical resonances. In our experience the benefits of aggressive skew are worth the complications for data analysis.

5.1 *Minimum detectable absorption (MDA)*

Most researchers cite a value for minimum detectable absorption, the 1σ value of some limiting noise level $\frac{\Delta P}{P}$ in a spectrum, normalized by total power P and integration time T_{i}:

$$\mathrm{MDA} = \left(\frac{\Delta P}{P}\right)_n \cdot \sqrt{T_{\mathrm{i}}} \quad \text{or} \quad \left(\frac{\Delta P}{P}\right)_n \cdot \frac{1}{\sqrt{BW}}\,, \tag{11}$$

where n is the number of scans integrated [27].

MDA can be interpreted in different ways, since since both $\Delta P/P$ and $\sqrt{T_{\mathrm{i}}}$ can be evaluated differently. $\Delta P/P$ can be taken as the 1σ residual along a laser scan after fitting, which includes small-scale but stationary baseline fluctuations, or it can be taken as the standard deviation of individual data points over time, which excludes stationary etalons. Neither interpretation is clearly "correct". Stationary etalons may affect fits even more strongly than does white noise.

The published literature also shows a difference of opinion on the appropriate time basis for an MDA calculation. One common interpretation of MDA is the measured deviation in a scan taken during real-world acquisition conditions for 1 s of integration, such that

$$\mathrm{MDA_{ps}} = \left(\frac{\Delta P}{P}\right)_n \sqrt{n} \cdot \sqrt{T_{\mathrm{scan}}}\,. \tag{12}$$

If the actual data from which $\Delta P/P$ is measured involve 1 s of integration, then $nT_{\mathrm{scan}} = 1$ s. Our term $\mathrm{MDA_{ps}}$ denotes "per scan" MDA. It is not a constant for a given instrument, because the integration time for each sampled point is a function of the scan length. The same instrument would yield a higher $\mathrm{MDA_{ps}}$ when scanning broadly over multiple lines than when scanning narrowly over a single one.

Some experimenters prefer a definition of MDA that is independent of scan characteristics, and use a "per point" MDA that refers to the minimum detectable absorption if integrating for 1 s on an individual datapoint rather than sweeping over an actual scan. $\mathrm{MDA_{pp}}$ is necessarily then less than $\mathrm{MDA_{ps}}$.

$$\mathrm{MDA_{pp}} = \left(\frac{\Delta P}{P}\right)_n \cdot \frac{1}{\sqrt{BW}}\,, \tag{13}$$

with BW variously taken as $1/n$ times the acquisition rate (or half that, the sampling bandwidth) or the detector bandwidth or the cavity bandwidth. If we denote all bandwidths as bw (so that $BW = bw/n$), then $\mathrm{MDA_{pp}}$ is lower than $\mathrm{MDA_{ps}}$ by a factor $\sqrt{bw/f_{\mathrm{scan}}}$. For typical ICOS instruments, this factor $\approx 15-45$. Note that if bw is taken as the acquisition rate, this factor is equal to the square root of the number of datapoints per spectrum, #pts:

$$\sqrt{bw/f_{\mathrm{scan}}} = \sqrt{n} \cdot \sqrt{T_{\mathrm{scan}}/\#\mathrm{pts}}\,, \tag{14}$$

so that

$$\mathrm{MDA_{pp}} = \mathrm{MDA_{ps}}/\sqrt{\#\mathrm{pts}}\,. \tag{15}$$

5.2 *Noise equivalent absorption sensitivity (NEAS)*

A second commonly cited metric of instrument performance is NEAS, the minimum detectable absorption scaled to pathlength, which is generally given as a "per bandwidth" or "per point" value.

$$\mathrm{NEAS} = \left(\frac{\Delta P}{P}\right)_n \cdot \frac{1}{L_{\mathrm{eff}}} \cdot \frac{1}{\sqrt{BW}} \tag{16}$$

or

$$\mathrm{NEAS} = \frac{\mathrm{MDA_{pp}}}{L_{\mathrm{eff}}}\,, \tag{17}$$

where L_{eff} is the effective optical path and BW is any of the options listed above [27]. For an instrument involving a single source of white noise and a single detection bandwidth, the meaning of NEAS is clear. NEAS then allows comparison of intrinsic spectroscopic performance of instruments with different pathlengths or spectral scan lengths. For OA-ICOS and other techniques with multiple bandwidths, the definition of NEAS is ambiguous. The variety of interpretations of MDA_{pp} described above apply to NEAS as well.

Some authors (e.g. [6]) take the relevant bandwidth as the data acquisition rate $r_{\text{data}} = \#\text{pts}/T_{\text{scan}}$. In this case

$$\text{NEAS} = \frac{\text{MDA}_{\text{ps}}}{L_{\text{eff}} \cdot \sqrt{\#\text{pts}}}, \tag{18}$$

where MDA_{ps} is as previously defined (12). In this work, we use the sampling bandwidth, i.e. the Nyquist frequency $r_{\text{data}}/2$, yielding

$$\text{NEAS} = \frac{\text{MDA}_{\text{ps}} \cdot \sqrt{2}}{L_{\text{eff}} \cdot \sqrt{\#\text{pts}}}. \tag{19}$$

More commonly authors use the detection bandwidth (e.g. [7]) or the cavity bandwidth (e.g. [4]). Some argue that the relevant bandwidth is the lowest frequency in the system, but this practice is not always followed. The two experiments just cited have similar configurations and yet the authors interpret NEAS differently (with a factor of three implication).

5.3 *Comparison of reported values*

The diversity in optical configurations used in OA-ICOS frustrates attempts to create a single common metric by which to judge intrinsic performance. In Table 1 we list relevant parameters for a variety of published OA-ICOS experiments, adjusted in some cases to a common definition for comparison. We have rescaled MDA to "per scan" values to avoid the question of which bandwidth is relevant for a "per point" figure. "Per scan" values also give a more intuitive understanding of the instrument's performance in its normal operation, as no spectroscopic measurement is made on a single point. For NEAS, which is by definition a "per point" value, we have simply collected the published values (other than as discussed in the figure caption). It should be recognized, however, that NEAS values between experiments are not strictly comparable.

We suggest that future instrument and experiment descriptions use a metric which is more directly related to the purpose of these devices, the measurement of trace gases. Most experimenters do cite their 1σ measurement precision or minimum detectable gas concentration, a number that takes into account many of the relevant factors that affect a measurement, but precision is usually stated in units of the mixing ratio of the measured species (e.g. ppbv of CO). Readers cannot therefore compare experiments without running synthetic spectra. To facilitate comparison of quite different instruments, we suggest that precision also be stated as MDA_{meas}, the linecenter fractional absorption of a gas concentration equal to the 1σ measurement precision in 1 s integration.

Use of MDA_{meas} also facilitates understanding of instrument performance. The "fit factor" or ratio $\text{MDA}_{\text{meas}}/\text{MDA}_{\text{ps}}$ describes the efficacy of the spectral fit at deriving concentrations relative to baseline "noise" levels. A fit factor greater than 1 means that integrating across the line adds value. Harvard ICOS was designed for a "fit factor" of approximately 1 – for HDO, MDA_{meas} and MDA_{ps} are both 3.6×10^{-4} – with a rapid scan rate relative to f_{cav} producing only a few independent pieces of information across a spectral line. These conditions produced optimal measurement precision in this particular instrument. In experiments with lower $f_{\text{line}}/f_{\text{cav}}$, the fit factor may exceed 1 and citing MDA_{ps} alone may effectively understate measurement capability.

6 Conclusions

Even when sensitivity is the sole design criterion, design of an OA-ICOS instrument involves many tradeoffs between competing factors that impact instrument performance. The many OA-ICOS experiments of recent years, including the Harvard ICOS Isotope Instrument discussed here, show a wide range of design choices reflective of this series of compromises. Comparing these choices can inform the design of future experiments.

First, it is noteworthy that for all of the OA-ICOS experiments catalogued in Table 1, minimum detectable absorp-

Ref.	λ	NEAS ($\text{cm}^{-1}\text{Hz}^{-1/2}$)	MDA_{ps} ($\text{Hz}^{-1/2}$)	L_{eff} (m)	L (cm)	$1-R$ (ppm)	Laser	Power (mW)	τ (μs)	f_{cav} (kHz)	bw_{det} or f_{acq} (kHz)	f_{line} (kHz)	f_{scan} (Hz)	$\sim \tau_{\text{line}}/\tau$
[6]	1.565	2.7×10^{-12}	1.6×10^{-4}	27 500	110	40	DFB	30	91.7	2	15	0.7	30	3
this work	**6.738**	$\mathbf{2.4 \times 10^{-11}}$	$\mathbf{3.6 \times 10^{-4}}$	**4200**	**90**	**225**	**QC**	**35**	**13.4**	**12**	**160**	**4.0**	**113**	3
[4]	1.565	3.1×10^{-11}	1×10^{-4}	4200	70	165	DFB	10	14.1	11	30	0.1	200	90
[3]	0.631	1.8×10^{-10}	8.4×10^{-4}	2680	67	250	DFB	2–3	8.9	18	3	0.02	10	800
[7]	1.605	3.9×10^{-10}	1.3×10^{-4}	1400	28	160	DFB	10	5.8	27	90	0.6	460	45
[25]	1.573	5.0×10^{-9}	2.5×10^{-4}	68	44	4400	DFB	20	0.3	477	0.9	0.2	50	3000
[24]	3.38	5.7×10^{-9}	5.0×10^{-3}	1800	90	500	DFG	4	6.0	27	3	0.1	125	250

TABLE 1 Experimental parameters for various OA-ICOS studies and resulting derived sensitivities, taken from the published literature. Results from this work are boldfaced. Note the variety of parameter choices and sensitivities. In all cases MDA_{ps} is derived from published values of MDA_{pp} (or NEAS and L_{eff}), bandwidth, and scan rate (using $\text{MDA}_{\text{ps}} = \text{MDA}_{\text{pp}} \cdot \sqrt{bw/f_{\text{scan}}}$), and should be taken with some caution. NEAS values here are as published, except that of [6] where for consistency we use the analog sampling frequency instead of the digital acquisition rate, i.e. we adjust published NEAS upwards by $\sqrt{2}$. Spectral line FWHM and f_{line} are estimated by eye from published figures and are only approximate, as is the derived τ_{line}/τ. Some bandwidth values were provided by authors via personal communication. This table does not represent all work on OA-ICOS. The criterion for inclusion was that a paper contain sufficient information to determine calculate most relevant instrument parameters without generating synthetic spectra. Reporting of instrument performance is sufficiently non-standardized that many important papers are not included here

tion as defined here is not particularly impressive compared to traditional multipass experiments, the best of which can achieve MDA_{ps} a hundred times lower [26]. The combination of optical resonance effects and low throughput power leaves OA-ICOS spectra with relatively high baseline "noise". OA-ICOS is competitive with traditional multipass spectroscopy only because its extreme effective optical pathlengths produce increased signal – i.e. absorption depth for a particular gas sample – that can outweigh this effect. NEAS values in OA-ICOS, which are scaled by pathlength, can thus be low even though MDA_{ps} is not. OA-ICOS is not then the appropriate choice for all experimental situations, but is favored if per-pass absorption is small and mirror reflectivity correspondingly large.

Second, the experiments of Table 1 do vary in some parameters. The strongest differences lie in the scan rate relative to cavity bandwidth, τ_{line}/τ, with experimental choices varying by three orders of magnitude. The resultant NEAS values suggest that more aggressive scanning may be beneficial in OA-ICOS by suppressing the buildup of optical resonances that would otherwise hamper measurements made with ultra-reflective mirrors [6] or poor beam quality (this work), allowing low NEAS in the near- and mid-IR, respectively. This effect is not due solely to different definitions of NEAS; the two experiments remain outliers in their wavelength groups regardless of how NEAS is calculated.

It is not, however, possible to confirm a net experimental benefit of rapid scanning without a common metric for comparison of instrument performance. Scan rates for Harvard ICOS are chosen to yield MDA_{ps} essentially equal to MDA_{meas}, so that measurement precision is approximately that inferred from per-point "noise". In slow-scanning OA-ICOS experiments, multiple independent datapoints across an absorption feature can result in increased fit precision such that $MDA_{meas} < MDA_{ps}$. Comparison of MDA_{ps} alone can thus be misleading. NEAS introduces the further complication of multiple bandwidths. We urge the community to adopt a common standard of reporting MDA_{meas} and L_{eff} to permit ready comparison of instruments and understanding of design choice implications.

ACKNOWLEDGEMENTS We are grateful to V. Kasyutich and W. Zhao for helpful discussions on sensitivity metrics (though we also want to exempt them from responsibility for any opinions expressed in this article; those should be assigned to the authors alone). We also thank two anonymous reviewers. Funding for this work was provided in part by a NASA Instrument Incubator Program grant and a NOAA Postdoctoral Fellowship in Climate and Global Change.

REFERENCES

1 R. Engeln, G. Berden, R. Peeters, G. Meijer, Rev. Sci. Instrum. **69**, 3763 (1998)
2 A. O'Keefe, J.J. Scherer, J.B. Paul, Chem. Phys. Lett. **307**, 343 (1999)
3 J.B. Paul, L. Lapson, J.G. Anderson, Appl. Opt. **40**, 4904 (2001)
4 D.S. Baer, J.B. Paul, J.B. Gupta, A. O'Keefe, Appl. Phys. B **75**, 261 (2002)
5 Y.A. Bakhirkin, A.A. Kosterev, C. Roller, R.F. Curl, F.K. Tittel, Appl. Opt. **43**, 2257 (2004)
6 G.S. Engel, W.S. Drisdell, F.N. Keutsch, E.J. Moyer, J.G. Anderson, Appl. Opt. **45**, 9221 (2006)
7 V.L. Kasyutich, P.A. Martin, R.J. Holdsworth, Appl. Phys. B **85**, 413 (2006)
8 Y.A. Bakhirkin, A.A. Kosterev, R.F. Curl, F.K. Tittel, D.A. Yarekha, L. Hvozdara, M. Giovannini, J. Faist, Appl. Phys. B **82**, 149 (2006)
9 H.J. Jost, A. Castrillo, H. W. Wilson, Isot. Environ. Health Stud. **42**, 37 (2006)
10 M.R. McCurdy, Y.A. Bakhirkin, F.K. Tittel, Appl. Phys. B **85**, 445 (2006)
11 E.R. Crosson, K.N. Ricci, B.A. Richman, F.C. Chilese, T.G. Owano, R.A. Provencal, M.W. Todd, J. Glasser, A.A. Kachanov, B.A. Paldus, T.G. Spence, R.N. Zare, Anal. Chem. **74**, 2003 (2002)
12 E.R.T. Kerstel, G. Gagliardi, L. Gianfrani, H.A.J. Meijer, R. van Trigt, R. Ramaker, Spectrochim. Acta A **58**, 2389 (2002)
13 J.B. McManus, M.S. Zahniser, D.D. Nelson, L.R. Williams, C.E. Kolb, Spectrochim. Acta A **58**, 2465 (2002)
14 J.B. McManus, D.D. Nelson, J.H. Shorter, R. Jimenez, S. Herndon, S. Saleska, M. Zahniser, J. Mod. Opt. **52**, 2309 (2005)
15 A.J. Schauer, M.J. Lott, C.S. Cook, J.R. Ehleringer, Rapid Commun. Mass Spectrom. **19**, 359 (2005)
16 E.R.T. Kerstel, R.Q. Iannone, M. Chenevier, S. Kassi, H.J. Jost, D. Romanini, Appl. Phys. B **85**, 397 (2006)
17 T.J. Griffis, J.M. Baker, S.D. Sargent, B.D. Tanner, J. Zhang, Agric. For. Meteorol. **124**, 15 (2004)
18 G. Lis, L.I. Wassenaar, M.J. Hendry, Anal. Chem. **80**, 287 (2008)
19 B. Tuzson, M.J. Zeeman, M.S. Zahniser, L. Emmenegger, Infrared Phys. Technol. **51**, 198 (2008)
20 D.S. Sayres, E.J. Moyer, T.F. Hanisco, J.M. St. Clair, F.N. Keutsch, A. O'Brien, N.T. Allen, L. Lapson, J.N. Demusz, M. Rivero, T. Martin, M. Greenberg, C. Tuozzolo, G.S. Engel, J.H. Kroll, J. Paul, J.G. Anderson, in preparation for Rev. Sci. Instrum.
21 D.R. Herriott, H.J. Schulte, Appl. Opt. **4**, 883 (1965)
22 J. Morville, D. Romanini, M. Chenevier, A. Kachanov, Appl. Opt. **41**, 6980 (2002)
23 L.S. Rothman, A. Barbe, D.C. Benner, L.R. Brown, C. Camy-Peyret, M.R. Carleer, K. Chance, C. Clerbaux, V. Dana, V.M. Devi, A. Fayt, J.M. Flaud, R.R. Gamache, A. Goldman, D. Jacquemart, K.W. Jucks, W.J. Lafferty, J.Y. Mandin, S.T. Massie, V. Nemtchinov, D.A. Newnham, A. Perrin, C.P. Rinsland, J. Schroeder, K.M. Smith, M.A.H. Smith, K. Tang, R.A. Toth, J. Vander Auwera, P. Varanasi, K. Yoshino, J. Quant. Spectrosc. Radiat. Transf. **82**, 5 (2003)
24 P. Malara, P. Maddaloni, G. Gagliardi, P. De Natale, Opt. Express **14**, 1304 (2006)
25 W. Zhao, X. Gao, W. Chen, W. Zhang, T. Huang, T. Wu, H. Cha, Appl. Phys. B **86**, 353 (2007)
26 P. Weibring, D. Richter, J.G. Walega, A. Fried, Opt. Express **15**, 13476 (2007)
27 F.K. Tittel, D. Richter, A. Fried, Mid-infrared laser applications in spectroscopy. In: *Solid-State Mid-Infrared Laser Sources*, Vol. 89 of *Topics in Applied Physics* (Springer, Berlin, 2003) pp. 445–510